Electronic Supplementary Material (ESI) for Physical Chemistry Chemical Physics.

Electronic Supplementary Information (ESI)

Thermal Correction Procedure

The equations governing temperature rise under EHL conditions were first described by Archard.[42]

There are two components, the 'flash temperature rise', $\Delta\bar{T}_{surf}$, of the solid surfaces in response to transient heat input as they traverse the contact, and an additional rise of oil film temperature above that of the bounding solid surfaces, $\Delta\bar{T}_{oil}$, due to the relatively low thermal conductivity of the oil.

The total mean temperature rise of the oil film above the inlet temperature is then given, for a point contact, by:

$$\Delta\bar{T}_{tot} = \Delta\bar{T}_{surf} + \Delta\bar{T}_{oil}$$

$$\Delta\bar{T}_{tot} = \left(\frac{1}{(2\pi K_s \rho c)^{0.5}} t_i^{0.5} h + \frac{1}{8K_{oil}} h^2\right)\bar{\tau}\,\dot{\gamma} \qquad \text{(Equation 3)}$$

where the first term describes the mean flash temperature rise and the second the additional mean oil film temperature rise. In Equation 3, K_s, ρ and c the thermal conductivity, density and specific heat of the solid bodies, respectively, t_i is the time of transit of the surfaces across the contact, h the film thickness and K_{oil} the thermal conductivity of the oil at the mean pressure of the contact, $\bar{\tau}$ is the mean shear stress and $\dot{\gamma}$ is the strain rate. The flash temperature term in Equation 3 assumes that both solids are of the same material and travel at approximately the same speed with respect to the contact, but it can quite easily be adjusted to accommodate different materials and speeds. In the second term, the value in the denominator (8) is debated and depends on where heat is generated in the oil film. Archard derived the value of 8 assuming that heat is generated evenly through the oil film thickness (i.e. Couette flow), while a value of 4 was obtained if all the heat is generated at the midplane (i.e. central localisation).[1,42]

Equation 3 shows that at high values of shear stress and strain rate, the mean oil film temperature can rise very significantly, particularly when the film thickness, h, is large. This complicates the interpretation of traction curves since it must be accounted for before any model of rheology can be inferred.[1] To achieve this, we assume a mean temperature rise across the contact, Johnson and Greenwood have demonstrated the validity of the mean temperature approach.[43] We start with a set of mean shear stress versus strain rate curves made at a series of different bulk temperatures between 30 and 120 °C (*e.g.* Figure S1). Note that in Figure S1, the 110 and 120 °C data are not shown since we do not determine a thermal correction at these temperatures as this would involve extrapolation.[44] Our correction of the experimental shear stress measurements involves two stages.[1,44]

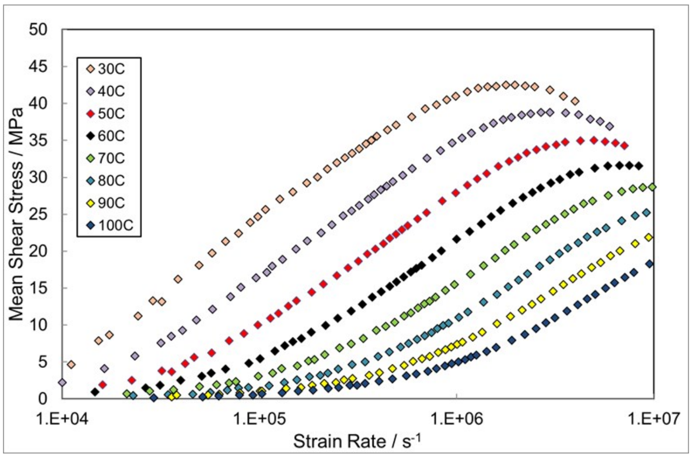

Figure S1. Mean shear stress *versus* strain rate for squalane at 0.75 GPa (50 N, steel/steel) with different bulk oil temperatures

In the first stage, we use Equation 3 to estimate the mean temperature rise for every single measurement, based on the mean shear stress and strain rate of this measurement; thus, for each measured data point, we now have a corrected mean film temperature which is equal to or higher than the bulk test temperature.[44]

In the second stage, for all shear stress data points, we identify its strain rate and extract, from the data measured at other temperatures, measurements made at this identical strain rate (with interpolation when necessary). We thus obtain a plot of mean shear stress versus corrected mean temperature at this fixed strain rate (see for example Figure 1 in reference[44]). We fit a smooth curve to this and use interpolation to determine, for each data point, how much the mean shear stress will have been reduced by the calculated rise in temperature. We then add this value to the measured mean shear stress. When carried out on all points in a shear stress *versus* log(strain rate) curve, this gives us an isothermal mean shear stress *versus* log(strain rate) curve at the bulk test temperature. We only do this for mean temperature rises of <10°C, since we recognise that the procedure becomes less exact as temperature rise increases.[44]

It is important to note that this procedure makes no assumptions about the rheology of the film nor how mean shear stress varies with temperature. Instead, the latter is extracted directly from our measurements made at a series of different temperatures. The thermally-corrected mean shear stresses calculated using this interpolation method are very similar to those calculated using a 3-D fitting procedure.[3]

Fluid Force-Field Parameters

Interactions between the liquid molecules are represented with an updated form of the all-atom 'optimized potential for liquid simulations' force-field,[55] L-OPLS-AA.[56] In this force-field, both bonded and non-bonded parameters have been updated for several atom types to provide a more realistic description of long-chain alkanes[56] and, more recently, alcohols and esters.[57] Specifically, parameters for all primary and secondary carbon atoms and aliphatic hydrogen atoms in squalane, DEHS, DCMP and DM2H were taken from reference[56]. Tertiary and quaternary carbon atoms have the same Lennard-Jones parameters as primary and secondary carbon atoms,[56] with their partial charges adjusted to ensure that the molecules have no overall charge. Parameters for the ester group in DEHS are taken from reference[57].

In order to be confident that the force-field was suitable for the molecules chosen in this study, it was ensured that their experimental liquid density, ρ, was accurately reproduced in bulk simulations of 100 molecules in the isothermal-isobaric (NPT) ensemble (see reference[60] for full methodology). Table S1 shows that the experimental and simulated densities are in good agreement, confirming the suitability of chosen force-field for the studied fluids.

Table S1. Experimental and simulated densities of the studied fluids, high pressure data is from references[38,39], ambient data was measured using an Anton Paar Density Meter

Fluid	**T / °C**	**P / GPa**	**Experimental ρ / g cm^{-3}**	**Simulated ρ / g cm^{-3}**	**Simulation Error / %**
Squalane	20	0.796	0.976	0.960	-1.7
	20	0.875	0.984	0.967	-1.8
	20	0.955	0.991	0.974	-1.7
	8	0.955	0.995	0.978	-1.7
	25	0.000101	0.810	0.812	0.2
DM2H	25	0.000101	0.961	0.972	1.1
DCMP	25	0.000101	0.890	0.901	1.2
DEHS	25	0.000101	0.914	0.926	1.3

Boundary Slip

Boundary slip occurs when the fluid cohesion is relatively stronger than its adhesion to the solid slabs,[52] meaning that the slabs do not transfer sufficient momentum to shear the fluid.[46] The phenomenon is commonly observed in NEMD simulations of very thin films (<10 nm) between atomically smooth slabs.[46–50] The slip length has been shown to increase with increasing; fluid viscosity, wall stiffness, sliding velocity, and pressure.[46–50] Conversely, the slip length has been shown to decrease with increasing surface-fluid interaction strength and film thickness[47–49] and to be virtually eliminated in the presence of atomic-scale surface roughness.[51]

Boundary slip has been observed experimentally for viscous polybutadiene between oleophobic surfaces;[33] however, this phenomenon is not expected to occur for the fluids, surfaces, and experimental conditions used in the current study (Table 1).[2,6] Large-scale NEMD simulations of a >100 nm *n*-hexane film between iron surfaces under realistic EHL conditions (F_N = 1 GPa, $\dot{\gamma}$ = 10^5 s^{-1}) confirmed the suitability of a macroscopic no-slip boundary condition for this system.[48] However, these simulations were extremely computationally expensive, making them unsuitable for the wide parameter study required here. Therefore, in order to increase computational efficiency, most of the NEMD simulations were performed on the thinnest systems (h ≈ 15 nm) for which boundary slip did not occur under the conditions of interest on the wetting[9] α-Fe_2O_3 slabs.

The parameters used for the α-Fe_2O_3 slabs were similar to those developed by Savio et al.[46] and Berro et al.[53]; ε_O = 0.21 kcal mol^{-1}, σ_O = 2.96 Å, q_O = -0.514 e; ε_{Fe} = 20.0 kcal mol^{-1}, σ_{Fe} = 2.32 Å, q_{Fe} = +0.771 e. The value of ε_{Fe} was increased relative to these previous studies to increase the strength of short-ranged surface-fluid interactions and discourage boundary slip, allowing a computationally-feasible film thickness to be simulated for this extensive parameter study. It is important to note that previous NEMD studies have shown that, once slip is prevented, an increase in the strength of surface-fluid interactions does not significantly affect the shear stress in the confined fluid.[46,53]

Film Thickness

Apart from in very strongly confined systems,[11] and in the absence of boundary slip, the shear stress in bulk and confined simulations is virtually indistinguishable.[7,46,52] In order to ensure that the choice of film thickness in the NEMD simulations did not significantly influence the mean shear stress results, some systems were also tested in systems with half and double the film thickness. Figure S2 shows the variation in the block-averaged shear stress and pressure with sliding distance for three different film thicknesses for a representative case (squalane at 0.5 GPa, 80 °C, 3.1 x 10^8 s^{-1}). These systems all gave the same shear stress result at equal strain rate within the statistical uncertainty. This confirms that the shear stress measurements from the NEMD simulations (h ≈ 15 nm) are directly comparable to results from the thicker experimental films (h ≈ 150 nm).

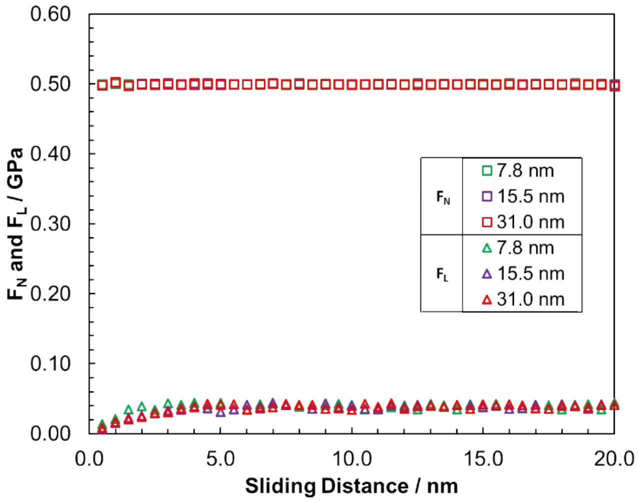

Figure S2. Example of the variation in the block-averaged shear stress (F_L) and pressure (F_N) with sliding distance for squalane systems with film thicknesses of 7.75 nm (2.5 m s^{-1}), 15.5 nm (5 m s^{-1}) and 31.0 nm (10 m s^{-1}) at 3.1 x 10^8 s^{-1}, 0.5 GPa, 80 °C

Additional Velocity Profiles

Figure S3 shows how the *x*-velocity profile in the *z*-dimension, $\mathrm{v}_x(z)$, and the atomic mass density profile in the *z*-dimension, changes with the applied pressure for DEHS. The profiles show similar flow behaviour as observed for the other lubricant, squalane (Figure 6).

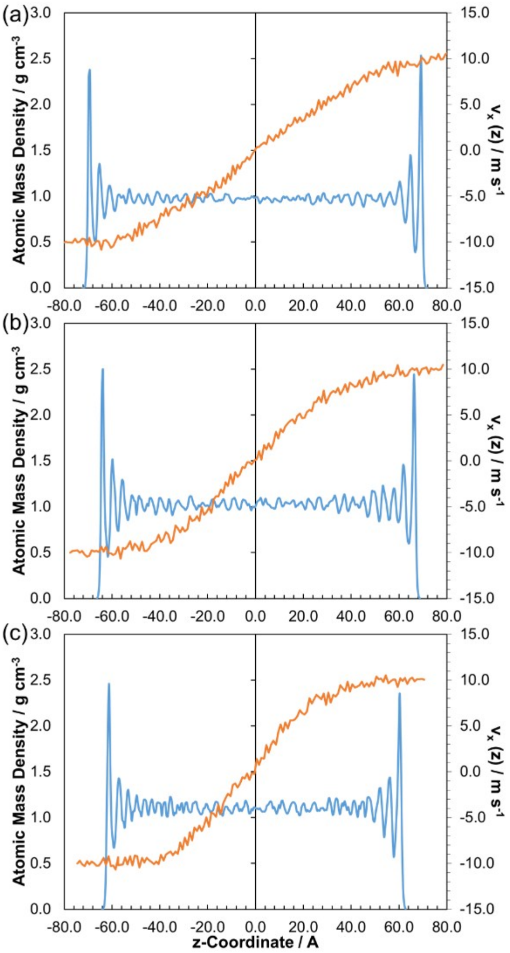

Figure S3. Atomic mass density (blue) and velocity (orange) profiles for DEHS at: 80 °C, 20 m s^{-1} ($\dot{\gamma} \approx 10^9$ s^{-1}), and; 0.50 GPa (a), 1.00 GPa (b), 2.00 GPa (c). Time-averaged for the final 5 nm of sliding.

Figure S4 shows how the *x*-velocity profile in the *z*-dimension, $v_x(z)$, and the atomic mass density profile in the *z*-dimension, changes with the applied pressure for DCMP. The profiles show similar flow behaviour as observed for the other traction fluid, DM2H (Figure 7). However, at the lowest pressure considered (0.5 GPa), the flow is more Couette-like for DCMP (Figure S4) than DM2H (Figure 7).

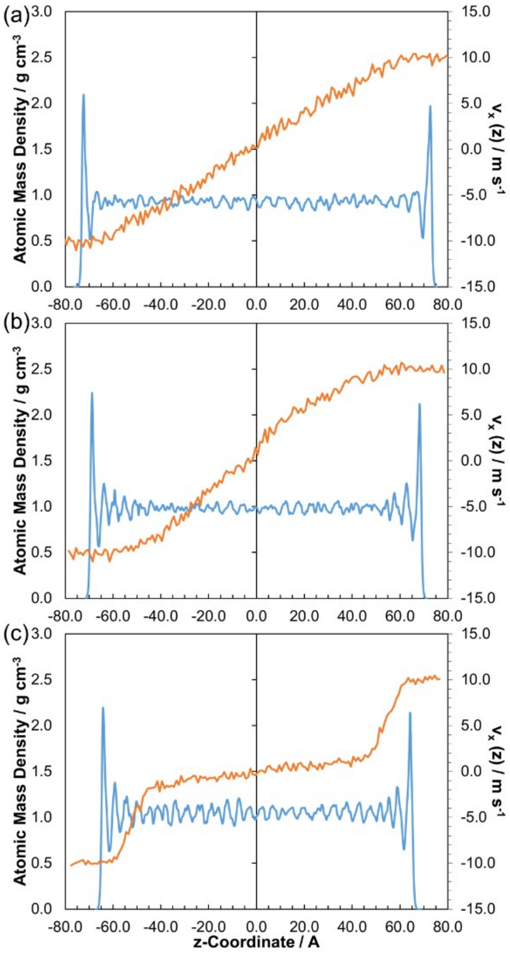

Figure S4. Atomic mass density (blue) and velocity (orange) profiles for DCMP at: 80 °C, 20 m s^{-1} ($\dot{\gamma} \approx 10^9$ s^{-1}), and; 0.50 GPa (a), 1.00 GPa (b), 2.00 GPa (c). Time-averaged for the final 5 nm of sliding.

Graphical Abstract

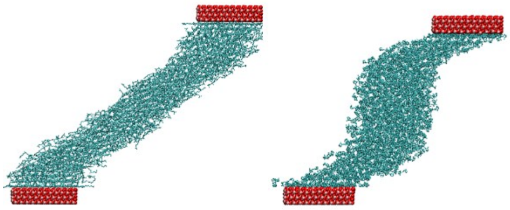

Novelty statement

Atomistic simulations and tribology experiments uncover the effect of molecular structure on the flow and friction behaviour of confined films under extreme conditions.